THE JOURNAL OF PHYSICAL CHEMISTRY Letters

Letter

pubs.acs.org/JPCL

High Capacity MoO_2/Graphite Oxide Composite Anode for Lithium-Ion Batteries

Yun Xu,[†] Ran Yi,[‡] Bin Yuan,[†] Xiaofei Wu,[†] Marco Dunwell,[†] Qianglu Lin,[†] Ling Fei,[†] Shuguang Deng,[†] Paul Andersen,[†] Donghai Wang,*,[‡] and Hongmei Luo*,[†]

[†]Department of Chemical Engineering, New Mexico State University, Las Cruces, New Mexico 88003, United States

[‡]Department of Mechanical & Nuclear Engineering, Penn State University, University Park, Pennsylvania 16802, United States

Ⓢ *Supporting Information*

ABSTRACT: Nanostructured MoO_2/graphite oxide (GO) composites are synthesized by a simple solvothermal method. X-ray diffraction and transmission electron microscopy analyses show that with the addition of GO and the increase in GO content in the precursor solutions, MoO_3 rods change to MoO_2 nanorods and then further to MoO_2 nanoparticles, and the nanorods or nanoparticles are uniformly distributed on the surface of the GO sheets in the composites. The MoO_2/GO composite with 10 wt % GO exhibits a reversible capacity of 720 mAh/g at a current density of 100 mA/g and 560 mAh/g at a high current density of 800 mA/g after 30 cycles. The improved reversible capacity, rate capacity, and cycling performance of the composites are attributed to synergistic reaction between MoO_2 and GO.

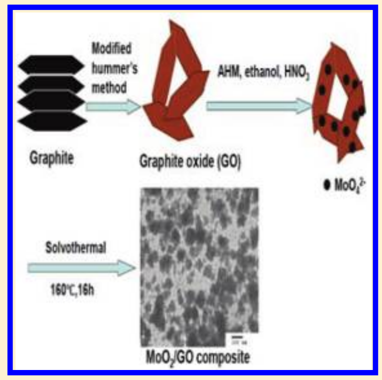

SECTION: Nanoparticles and Nanostructures

Nowadays, rechargeable lithium-ion batteries are widely used in mobile devices, hybrid, plug-in hybrid, and electric vehicles. The performance of batteries strongly depends on the electrode properties. A great effort has been made to synthesize a variety of electrode materials to improve the energy density, rate capability, and cycling stability.[1−3] Graphite has been commonly used as anode material, but it shows low theoretical specific capacity of 372 mAh/g due to the limit of thermodynamic equilibrium saturation composition of LiC_6.[4] Transition-metal oxides, such as Co_3O_4, MoO_3, and Fe_2O_3 are capable of combining 6 Li per formula unit,[5−9] corresponding to a much higher capacity than that of graphite. However, most metal oxides have poor electrical conductivity. In addition, during the cycling of Li insertion/extraction, metal oxides typically break into small metal clusters, resulting in a large volume expansion and a loss of capacity.[6]

Recently, nanostructured materials have received much attention as battery electrodes due to the short transport lengths for both electrons and Li ions, higher electrode-electrode contact area, and better accommodation of the strain of Li insertion/extraction.[10,11] For example, nanostructured Fe_2O_3, SnO_2, and Co_3O_4 anodes have been reported to improve the reversible capacity and rate capacity.[9,11−13] In addition, various carbon additives have also been coupled to the metal oxide nanoparticles to improve their conductivity. Graphene and reduced graphite oxide (RGO) are the most commonly used carbon matrix for the anode composite due to their excellent electronic conductivity, large surface area, flexibility, and chemical stability. A number of metal oxide/graphene and metal oxide/RGO hybrids or nanocomposites have been reported, including Fe_3O_4, Mn_3O_4, Co_3O_4, SnO_2, TiO_2, and NiO, in which metal oxides are distributed onto the surface of graphene or between the graphene layers, with performance better than that of their counterparts in terms of electrode capacity and cycling stability.[14−21]

MoO_2 can take 4 Li, corresponding to a high theoretical capacity of 838 mAh/g.[22] The mesoporous MoO_2 has a capacity of 750 mAh/g after 20 cycles at a current density of ∼35 mA/g.[23] The MoO_2/C hybrid nanowires deliver a capacity of 500, 400, or 300 mAh/g after 20 cycles at 200, 500, or 1000 mA/g, respectively.[24] The recently reported MoO_2/graphene gives a capacity of ∼420 mAh/g after 30 cycles but reaches 597 mAh/g after 70 cycles at 1000 mA/g.[21] Low-temperature solution routes have been developed for synthesis of MoO_2 nanostructures.[25−29] However, few MoO_2 nanostructures fabricated under mild conditions have been studied as high-performance anode materials. In this letter, we report MoO_2/graphite oxide (GO) nanocomposites prepared by a low-temperature solvothermal method for lithium battery anodes. Herein, GO was used as a metal oxide support without further reduction because MoO_2 is a metallic conductor.

GO was synthesized from natural graphite by a modified Hummers method.[30,31] In brief, 1 g of graphite powder (MTI, carbon content 99.9 to 99.99%) and 1 g of $NaNO_3$ (Aldrich,

Received: December 8, 2011
Accepted: January 12, 2012
Published: January 12, 2012

>99%) were mixed and put into concentrated 24 mL of H_2SO_4 (Sigma-Aldrich, 98%) in an ice bath; then, 6 g of $KMnO_4$ (Sigma-Aldrich, 99.6%) was added gradually and the mixture was stirred at 35 °C in a water bath for 18 h. Subsequently, the solution was slowly added to 300 mL of H_2O; then, 5 mL of 30% H_2O_2 (Sigma-Aldrich) was added. After continuously stirring for 2 h, the mixture was filtered and washed with 10% HCl aqueous solution (Sigma-Aldrich), DI water, and ethanol (Sigma-Aldrich, anhydrous). Finally, the GO powder was dispersed in 100 mL of H_2O.

The MoO_2/GO composite was prepared by a solvothermal method. First, 1 g of ammonium heptamolybdate (AHM) was dissolved in 50 mL of ethanol. Then, 6 mL of HNO_3 (Sigma-Aldrich, 70%) and various volumes of GO water solution (10 mg/mL, 0, 1, 3, 5, 7, and 9 mL) were added sequentially under vigorously stirring. The mixture was then transferred into a Teflon-lined stainless-steel autoclave. The reaction was maintained at 160 °C for 16 h. Finally, the product was rinsed with distilled water and dried at 100 °C. MoO_2 nanoparticles were prepared under the same conditions using AHM, HNO_3, and ethylene glycol as precursors and solvents.

The phase and structure of the GO, MoO_2, MoO_3, MoO_3/GO, and MoO_2/GO composites were characterized by X-ray diffraction (XRD) using Cu radiation on a powder Scintag XRD operating at 45 kV and 36 mA. The morphology and microstructure were investigated by H-7650 transmission electron microscopy (TEM). The GO content in the MoO_2/GO composites was determined by Pyris 1 TGA thermogravimetric analyzer (Perkin-Elmer). Raman spectroscopy was performed using the 632.8 nm (1.96 eV) laser excitation. The Brunauer–Emmett–Teller (BET) specific surface area of the samples was determined by an ASAP 2010 using the standard N_2 adsorption and desorption isotherm measurements at 77 K. The electrochemical experiments were performed using 2016 coin cells, which were assembled in an argon-filled dry glovebox (MBraun, Inc.) with the composite electrode as the working electrode and the Li metal as the counter electrode. The electrochemical performance was evaluated by galvanostatic charge/discharge cycling on an Arbin battery tester BT-2000 at room temperature under different current densities in the voltage range between 3.00 and 0.005 V versus Li^+/Li. The specific capacities were based on the mass of active material. MoO_2 or MoO_2/GO composites were mixed in a ratio of 80% active material, 10% super P (carbon additive), and 10% carboxymethyl cellulose (CMC).

As shown in Scheme 1, GO was first prepared from natural graphite by a modified Hummer's method[30,31] and dispersed in water to form a suspension of GO sheets (concentration of GO was 10 mg/mL). Then, various volumes of GO suspension were mixed with AHM, ethanol, and HNO_3; then, the mixture was solvothermally treated at 160 °C for 16 h to form the composites. XRD and TEM analyses show that rod-like or belt-like pure MoO_3 (JCPDS no.21-0569) was formed without GO in the solution (Figure S1 of the Supporting Information). The addition of 1 mL of GO suspension resulted in the formation of MoO_3/GO composite. With the further addition of 3 to 9 mL of GO suspension, MoO_2/GO composite was formed. Figure 1 shows the TEM images of GO and MoO_2/GO composites formed by adding 3, 5, and 9 mL of GO suspension in the solution and XRD patterns of MoO_3/GO and MoO_2/GO composites. As seen from Figure 1a, a curled morphology of GO sheets consisting of thin wrinkled structures was observed. For the composites, it is interesting to find that rod-like MoO_3 transforms to rod-like MoO_2 and further to nanoparticles of MoO_2 with increasing GO content, and MoO_2 nanorods or nanoparticles were dispersed on the surface of the GO sheets. In addition, the sizes of MoO_3 and MoO_2 decrease with the increase in GO amount, as determined from both XRD patterns and TEM images. For example, the MoO_2 rods obtained by adding 3 mL of GO suspension in the mixture are more than 200 nm long and ~150 nm in diameter. With 5 mL of GO suspension, the size of MoO_2 nanoparticles is 60–80 nm and decreases to <40 nm when 9 mL of GO suspension was added.

Scheme 1. Schematic Illustration of the Synthesis of the MoO_2/GO Composite

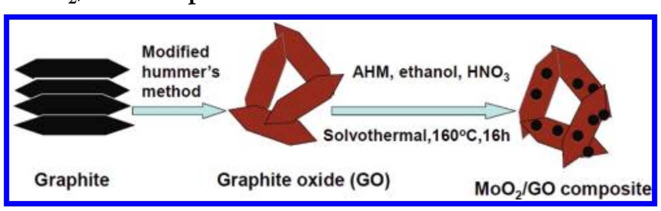

It is noted that poly(ethylene glycol), ethylene glycol, and alkali borohydrides have been reported as reducing agents for synthesizing MoO_2 in a hydrothermal process.[25−29] It is reasonable to point out that GO and ethanol could be reducing agents for forming MoO_2 in a hydrothermal process as well because MoO_3 is formed in the precursor solutions without GO. The Raman spectrum (Figure S2 of the Supporting Information) displayed both D-band and G-band in both pure GO and the composite, which indicates the existence of carbon in the composite. However, the ratio between the peak intensity I_D/I_G increases from 0.92 for the pure GO to 1.1 for the composite, indicating that the GO sheets were oxidized and became more disordered in the composite.[32] Therefore, GO (and ethanol) may function as reducing agents in the process. In the process, initially the MoO_4^{2-} ions (from precursor AHM) were attached to the highly hydrophilic surface of GO, and MoO_2 was formed by reduction MoO_4^{2-} in GO and ethanol atmosphere after solvothermal. GO sheets helped the dispersion of MoO_2 particles. MoO_2 nanoparticles were also prepared by using ethylene glycol as a solvent for comparison. The TEM image of MoO_2 is shown in Figure 1e. It can be seen that the morphology of the MoO_2 nanoparticles is similar to that of the MoO_2/GO composites, but MoO_2 nanoparticles tend to agglomerate. The XRD pattern is the same as the XRD pattern of MoO_2/GO composite shown in Figure 1f, indicating that the monoclinic structure MoO_2 (JCPDS no. 32-0671) and hexagonal structure MoO_2 (JCPDS no. 50-0739) coexist in the synthesized MoO_2 nanoparticles and the MoO_2/GO composites.

We first investigated the influence of GO content in the composites on battery performance. Figure 2a shows the capacity as a function of cycle numbers at a current density of 800 mA/g for three MoO_2/GO composites. The capacity of the composite with less GO (3 mL of GO suspension) showed capacities of 869 mAh/g at the second cycle and 246 mAh/g after 30 cycles. When we increased the amount of GO suspension to 9 mL, the composite showed a very low capacity of 190 mAh/g but with a stable performance with a capacity of 255 mAh/g after 30 cycles. However, the composite prepared by adding 5 mL of GO suspension showed a much higher capacity of 800 mAh/g at the second cycle and 563 mAh/g

dx.doi.org/10.1021/jz201619r | J. Phys. Chem.Lett. 2012, 3, 309−314

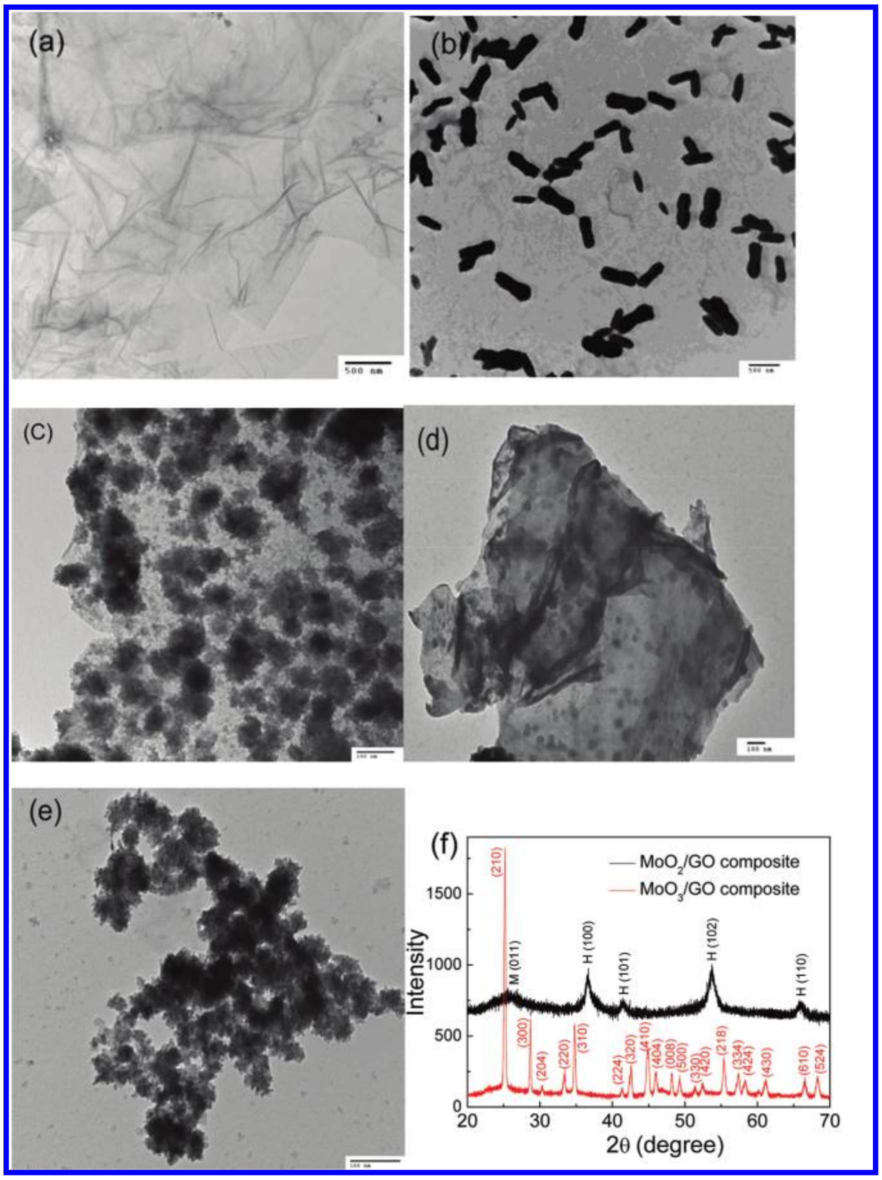

Figure 1. TEM images of (a) graphite oxide sheets, (b) MoO_2/GO composites prepared by adding 3 mL of GO solution, (c) MoO_2/GO composites prepared by adding 5 mL of GO solution, (d) MoO_2/GO composites prepared by adding 9 mL of GO solution, and (e) MoO_2 nanoparticles (scale bar: 500 nm in a and b; 100 nm in c−e). (f) XRD patterns of MoO_3/GO composite with 1 mL of GO in solution (MoO_3, JCPDS no.21−0569) and MoO_2/GO composite with 5 mL of GO in solution (monotonic MoO_2, JCPDS no. 32-0671; hexagonal MoO_2, JCPDS no. 50-0739).

after 30 cycles. TGA analysis shows that the GO weight percentages in the composites with 3, 5, and 9 mL of GO suspension are about 8, 10, and 14%. (See Figure S3 of the Supporting Information.) In other words, the capacity depends on the weight ratios of MoO_2 and GO in the composites as well as the morphology, and sizes of MoO_2 and GO play an important role in stabilizing the performance of the composite.

Figure 2b shows a charge and discharge profile of the composite with 10 wt % GO (5 mL GO suspension) for the 1st, 2nd, 5th, 10th, 20th, and 30th cycles at a current density of 100 mA/g and a voltage range of 3.00 and 0.005 V versus Li^+/Li. The discharge capacities of the anode in the 1st, 2nd, 5th, 10th, 20th, and 30th cycles are 1205, 926, 868, 815, 760, and 726 mAh/g, respectively. The charge capacities of the anode in the 2nd, 5th, 10th, 20th, and 30th cycles are 862, 848, 804, 746, and 712 mAh/g, respectively. The first-cycle irreversible capacity loss of 28.4% (from 1205 to 862 mAh/g) could be caused by the irreversible initial lithium consumption and the inevitable formation of solid electrolyte interface (SEI layer).[33−35] From the second cycle onward, 78.4% discharge capacity (from 926 to 726 mAh/g) and 82.6% charge capacity (from 862 to 712 mAh/g) are retained up to the 30th cycle with a Coulombic efficiency of 98%.

A comparison of the cycle performance between the MoO_2/GO composite (10 wt % GO in the composite) and the pure MoO_2 nanoparticles at a current density 100 mA/g is shown in Figure 2c. It was observed that the composite showed a much higher capacity than the pure MoO_2. The composite shows a discharge capacity of 926 mAh/g at the 2nd cycle and 726 mAh/g after 30 cycles. However, for the pure MoO_2 nanoparticles, only 352 mAh/g was achieved for the 2nd cycle, and ∼200 mAh/g was left after 30 cycles. On the basis of the calculation of capacity of the 30th cycle, the composite

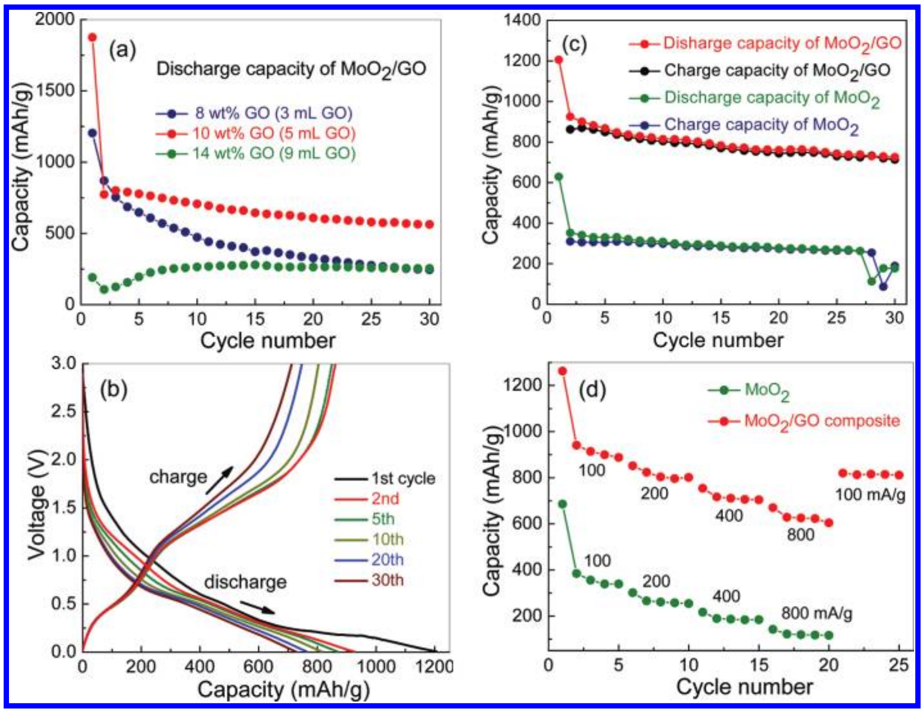

Figure 2. Electrochemical performance of the MoO_2/GO composites and MoO_2. (a) Cycling performance of MoO_2/GO composites prepared by adding 3, 5, and 9 mL of GO suspension, respectively, at a current density of 800 mA/g. (b) Discharge/charge voltage profiles of MoO_2/GO composite (with 5 mL of GO suspension) for the 1st, 2nd, 5th, 10th, 20th, and 30th cycle at a current density of 100 mA/g. (c) Cycling performance of pure MoO_2 and MoO_2/GO composite (with 5 mL of GO suspension) at a current density of 100 mA/g. (d) Rate performances of MoO_2 and MoO_2/GO composite (with 5 mL of GO suspension) between 0.005 and 3.00 V with increasing current density from 100 to 800 mA/g.

electrode takes 3.43 mols of Li, and the pure MoO_2 takes only 0.95 mols of Li.

The rate performance of the same composite and MoO_2 nanoparticles under increasing current densities of 100, 200, 400, and 800 mA/g is shown in Figure 2d. The composite shows a better rate performance than MoO_2. For example, the composite has a capacity of ~600 mAh/g even at a current density of 800 mA/g. The MoO_2 nanoparticles exhibit a capacity of only ~150 mAh/g. The cycle performance of pure GO at a current density of 100 mA/g (Figure S4 of the Supporting Information) shows that the GO capacity was a few tens initially and then dropped to 4−6 mAh/g immediately. The low capacity originates from the insulator property of GO, furthermore, without the spacer of MoO_2 nanoparticles, GO sheets easily stack together, which provides small host area for lithium ions.

Theoretically, MoO_2 has a specific capacity of 838 mAh/g, whereas the capacity of carbon material is 372 mAh/g. The theoretical capacity of the composite could be calculated as MoO_2 wt % × 838 mAh/g + carbon wt % × 372 mAh/g. The discharge capacities of MoO_2 measured at a current density of 100 mA/g in the first cycle (629 mAh/g) and the second cycle (352 mAh/g) are lower than the theoretical value of MoO_2. However, the discharge capacities of the composite measured at a current density of 100 mA/g in the first cycle (1205 mAh/g) and the second cycle (926 mAh/g) are much higher than the theoretical value (791.4 mAh/g for the composite consisting of 90 wt % MoO_2 and 10 wt % GO). The initial irreversible capacity results from the SEI formed in the first discharge process as well as the electrolyte decomposition at a low potential region around 0.3 V for the first cycle, as shown in Figure 2b. Hereafter, the extra capacity could arise from reversible reaction of lithium with the active surface groups including dangling C−H and C−OOH bonds on the surface of GO.[33−38] The improved performance may be attributed to synergistic interaction between the GO sheets and MoO_2 nanoparticles. For the composite, MoO_2 nanoparticles dispersed on the surface of GO sheets. GO may work as mechanical buffer that alleviates the volume change of the nanoparticles during charge and discharge.[39] Furthermore, the MoO_2 nanoparticles act as a spacer that prevents the GO sheets from agglomerating.[40] The possible reaction for the composite is

$$\begin{aligned} &MoO_{2+x} + (4 + 2x)Li^+ + (4 + 2x)e^- \\ &\quad \leftrightarrow Mo + 2Li_2O_{(MoO_2)} + xLi_2O_{(\text{graphite oxide})} \end{aligned}$$

in which the Mo metal nanoparticles formed on the surface of the GO make the reaction highly reversible.[40−42] However, for the pure MoO_2 nanoparticles, they tend to agglomerate, which provides a much smaller surface area for the transportation of lithium ions. (BET surface area of MoO_2 is 34 m^2/g and the MoO_2/GO composite with 10 wt % GO has a BET surface area of 60 m^2/g.) It is noted that from the TEM images of the MoO_2/GO composites (Figure 1b−d), 10 wt % GO composite has a highest density of MoO_2 particles on the surface of GO sheets because this composite shows the best performance among the three composites, and it may further prove the synergistic interaction between the GO sheets and MoO_2 nanoparticles, as we discussed above.

In summary, we report a simple two-step process for fabricating MoO_2/GO composite as a high-performance anode material for Li-ion batteries. The best performance was obtained on the composite with ~10 wt % of GO. The composite exhibits a good capacity retention with 726 mAh/g after 30 cycles at a current density of 100 mA/g. It also delivers an excellent rate capability of 560 mAh/g at a high current density of 800 mA/g after 30 cycles. The composite showed a much better performance than the MoO_2 nanoparticles. The high capacity, good capacity retention, and high rate capability can be attributed to the structure of nanoparticle/GO sheet composites. The flexible structure of 2-D GO sheets and the strong interaction between MoO_2 nanoparticles and GO sheets in the composite are beneficial for efficiently preventing volume expansion/contraction and aggregation of MoO_2 during the charge/discharge process.

■ ASSOCIATED CONTENT

Supporting Information

TEM, TGA, Raman spectrum, XRD, and cycle performance. This material is available free of charge via the Internet at http://pubs.acs.org.

■ AUTHOR INFORMATION

Corresponding Author

*E-mail: dwang@psu.edu and hluo@nmsu.edu.

Notes

The authors declare no competing financial interest.

■ ACKNOWLEDGMENTS

H.L. acknowledges the funding support from New Mexico State University, New Mexico Consortium, and Los Alamos National Laboratory. D.W. acknowledges support from Penn State and the Assistant Secretary for Energy Efficiency and Renewable Energy, Office of Vehicle Technologies of the U.S. Department of Energy under contract no. DE-AC02-05CH11231, subcontract no. 6951378 under the Batteries for Advanced Transportation Technologies (BATT) Program.

■ REFERENCES

(1) Liu, J.; Xue, D. F. Hollow Nanostructured Anode Materials for Li-Ion Batteries. *Nanoscale Res. Lett.* **2010**, *5*, 1525−1534.

(2) Taberna, P. L.; Mitra, S.; Poizot, P.; Simon, P.; Tarascon, J. M. High Rate Capabilities Fe_3O_4-Based Cu Nano-Architectured Electrodes for Lithium-Ion Battery Applications. *Nat. Mater.* **2006**, *5*, 567−573.

(3) Ban, C. M.; Wu, Z. C.; Gillaspie, D. T.; Chen, L.; Yan, Y. F.; Blackburn, J. L.; Dillon, A. C. Nanostructured Fe_3O_4/SWNT Electrode: Binder-Free and High-Rate Li-Ion Anode. *Adv. Mater.* **2010**, *22*, E145−E149.

(4) Dresselhaus, M. S.; Dresselhaus, G. Intercalation Compounds of Graphite. *Adv. Phys.* **2002**, *51*, 1−186.

(5) Lee, S. H.; Kim, Y. H.; Deshpande, R.; Parilla, P. A.; Whitney, E.; Gillaspie, D. T.; Jones, K. M.; Mahan, A. H.; Zhang, S. B.; Dillon, A. C. Reversible Lithium-Ion Insertion in Molybdenum Oxide Nanoparticles. *Adv. Mater.* **2008**, *20*, 3627−3632.

(6) Poizot, P.; Laruelle, S.; Grugeon, S.; Dupont, L.; Tarascon, J. M. Nano-Sized Transition-Metal Oxides as Negative-Electrode Materials for Lithium-Ion Batteries. *Nature* **2000**, *407*, 496−499.

(7) Du, N.; Zhang, H.; Chen, B.; Wu, J. B.; Ma, X. Y.; Liu, Z. H.; Zhang, Y. Q.; Yang, D.; Huang, X. H.; Tu, J. P. Porous Co_3O_4 Nanotubes Derived From Co4(CO)12 Clusters on Carbon Nanotube Templates: A Highly Efficient Material for Li-Battery Applications. *Adv. Mater.* **2007**, *19*, 4505−4509.

(8) Chernova, N. A.; Roppolo, M.; Dillon, A. C.; Whittingham, M. S. Layered Vanadium and Molybdenum Oxides: Batteries and Electrochromics. *J. Mater. Chem.* **2009**, *19*, 2526−2552.

(9) Reddy, M. V.; Yu, T.; Sow, C. H.; Shen, Z. X.; Lim, C. T.; Subba Rao, G. V.; Chowdari, B. V. R. α-Fe_2O_3 Nanoflakes as an Anode Material for Li-Ion Batteries. *Adv. Funct. Mater.* **2007**, *17*, 2792−2799.

(10) Maier, J. Nanoionics: Ion Transport and Electrochemical Storage in Confined Systems. *Nat. Mater.* **2005**, *4*, 805−815.

(11) Arico, A. S.; Bruce, P. G.; Scrosati, B.; Tarascon, J. M.; Schalkwijk, W. V. Nanostructured Materials for Advanced Energy Conversion and Storage Devices. *Nat. Mater.* **2005**, *4*, 366−377.

(12) Han, Y. T.; Wu, X.; Ma, Y. L.; Gong, L. H.; Qu, F. Y.; Fan, H. Porous SnO_2 Nanowire Bundles for Photocatalyst and Li Ion Battery Applications. *J. CrystEngComm.* **2011**, *13*, 3506−3510.

(13) Li, C. C.; Yin, X. M.; Chen, L. B.; Li, Q. H.; Wang, T. H. High Capacity and Excellent Cycling Stability of Branched Cobalt Oxide Nanowires as Li-Insertion Materials. *Appl. Phys. Lett.* **2010**, *97*, 043501.

(14) Kim, H.; Kim, S. W.; Park, Y. U.; Gwon, H.; Seo, D. H.; Kim, Y.; Kang, K. SnO_2/Graphene Composite with High Lithium Storage Capability for Lithium Rechargeable Batteries. *Nano. Res.* **2010**, *3*, 813−821.

(15) Paek, S. M.; Yoo, E. J.; Honma, I. Enhanced Cyclic Performance and Lithium Storage Capacity of SnO_2/Graphene Nanoporous Electrodes with Three-Dimensionally Delaminated Flexible Structure. *Nano Lett.* **2009**, *9*, 72−75.

(16) Wang, D. H.; Choi, D. W.; Li, J.; Yang, Z. G.; Nie, Z. M.; Kou, R.; Hu, D. H.; Wang, C. M.; Saraf, L. V.; Zhang, J. G.; et al. Self-Assembled TiO_2−Graphene Hybrid Nanostructures for Enhanced Li-Ion Insertion. *ACS Nano* **2009**, *3*, 907−914.

(17) Zhang, L. S.; Jiang, L. Y.; Yan, H. J.; Wang, W. D.; Wang, W.; Song, W. G.; Guo, Y. G.; Wan, L. J. Monodispersed SnO_2 Nanoparticles on both Sides of Single Layer Graphene Sheets as Anode Materials in Li-Ion Batteries. *J. Mater. Chem.* **2010**, *20*, 5462−5467.

(18) Kamat, P. V. Graphene-Based Nanoarchitectures. Anchoring Semiconductor and Metal Nanoparticles on a two-Dimensional Carbon Support. *J. Phys. Chem. Lett.* **2010**, *1*, 520−527.

(19) Wang, H. L.; Cui, L. F.; Yang, Y.; Casalongue, H. S.; Robinson, J. T.; Liang, Y.; Cui, Y.; Dai, H. J. Mn_3O_4−Graphene Hybrid as a High-Capacity Anode Material for Lithium Ion Batteries. *J. Am. Chem. Soc.* **2010**, *132*, 13978−13980.

(20) Zou, Y. Q.; Wang, Y. NiO Nanosheets Grown on Graphene Nanosheets as Superior Anode Materials for Li-Ion Batteries. *Nanoscale* **2011**, *3*, 2615−2620.

(21) Sun, Y.; Hu, X.; Luo, W.; Huang, Y. Self-Assembled Hierarchical MoO_2/graphene Nanoarchitectures and Their Application as a High-Performance Anode Material for Lithium-ion Batteries. *ACS Nano* **2011**, *5*, 7100−7107.

(22) Wang, Z. Y.; Chen, J. S.; Zhu, T.; Madhavi, S.; Lou, X. W. One-Pot Synthesis of Uniform Carbon-Coated MoO_2 Nanospheres for High-Rate Reversible Lithium Storage. *Chem. Commun.* **2010**, *46*, 6906−6908.

(23) Shi, Y. F.; Guo, B. K.; Corr, S. A.; Shi, Q. H.; Hu, Y. S.; Heier, K. R.; Chen, L. Q.; Seshadri, R.; Stucky, G. D. Ordered Mesoporous Metallic MoO_2 Materials with Highly Reversible Lithium Storage Capacity. *Nano Lett.* **2009**, *9*, 4215−4220.

(24) Gao, Q. S.; Yang, L. C.; Lu, X. C.; Mao, J. J.; Zhang, Y. H.; Wu, Y. P.; Tang, Y. Synthesis, Characterization and Lithium-Storage Performance of MoO_2/Carbon Hybrid Nanowires. *J. Mater. Chem.* **2010**, *20*, 2807−2812.

(25) Liang, Y.; Yang, S.; Yi, Z.; Sun, J.; Zhou, Y. Low Temperature Synthesis of a Stable MoO_2 as Suitable Anode Materials for Lithium Batteries. *Mater. Sci. Eng., B* **2005**, *121*, 153−156.

(26) Khorasani, M. M.; Norouzifar, M.; Shahrousvand, H. A New Reduction Route for the Synthesis of Nanoscale Metals and Metal Oxides with Ascorbic Acid at Low Temperature. *J. Iran. Chem. Soc.* **2010**, *7*, 113−122.

(27) Wang, S. T.; An, C. H.; Zhang, Y. G.; Zhang, Z. D.; Qian, Y. T. Ethanothermal Reduction to MoO_2 Microspheres via Modified Pechini Method. *J. Cryst. Growth* **2006**, *293*, 209−215.

(28) Chen, X. Y.; Zhang, Z. J.; Li, X. X.; Shi, C. W.; Li, X. L. Selective Synthesis of Metastable MoO_2 Nanocrystallites through a Solution-Phase Approach. *Chem. Phys. Lett.* **2006**, *418*, 105−108.

(29) Chen, J. L.; Burger, C.; Krishnan, C. V.; Chu, B. Morphogenesis of Highly Ordered Mixed-Valent Mesoporous Molybdenum Oxides. *J. Am. Chem. Soc.* **2005**, *127*, 14140−14141.
(30) Hummers, W. S.; Offeman, R. E. Preparation of Graphitic Oxide. *J. Am. Chem. Soc.* **1958**, *80*, 1339−1339.
(31) Zhu, X. J.; Zhu, Y. W.; Murali, S.; Stoller, M. D.; Ruoff, R. S. Nanostructured Reduced Graphene Oxide/Fe_2O_3 Composite as a High-Performance Anode Material for Lithium Ion Batteries. *ACS Nano* **2011**, *5*, 3333−3338.
(32) Lian, P. C.; Zhu., X. F.; Liang, S. Z.; Li, Z.; Yan, W. S.; Wang, H. H. Large Reversible Capacity of High Quality Graphene Sheets as an Anode Material for Lithium-Ion Batteries. *Electrochim. Acta* **2010**, *55*, 3909−3914.
(33) Courtney, I. A.; Dahn, J. R. Electrochemical and In Situ X-Ray Diffraction Studies of the Reaction of Lithium with Tin Oxide Composites. *J. Electrochem. Soc.* **1997**, *144*, 2045−2052.
(34) Ein-Eli, Y. Electrochem. A New Perspective on the Formation and Structure of the Solid Electrolyte Interface at the Graphite Anode of Li-Ion Cells. *Solid State. Lett.* **1999**, *2*, 212−214.
(35) Kang, Y. M.; Kim, K. T.; Lee, K. Y.; Lee, S. J.; Jung, J. H.; Lee, J. Y. Improvement of Initial Coulombic Efficiency of Co_3O_4 by Ballmilling Using Ni as an Additive. *J. Electrochem. Soc.* **2003**, *150*, A1538−A1543.
(36) Ji, X. L.; Herle, P. S.; Rho, Y.; Nazar, L. F. Carbon/MoO_2 Composite Based on Porous Semi-Graphitized Nanorod Assemblies from In Situ Reaction of Tri-Block Polymers. *Chem. Mater.* **2007**, *19*, 374−383.
(37) Dahn, J. R.; Zheng, T.; Liu, Y.; Xue, J. S. Mechanisms for Lithium Insertion in Carbonaceous Materials. *Science* **1995**, *270*, 590−593.
(38) Liu, T.; Luo, R. Y.; Yoon, S. H.; Mochida, I. Effect of Vacuum Carbonization Treatment on the Irreversible Capacity of Hard Carbon Prepared from Biomass Material. *Mater. Lett.* **2010**, *64*, 74−76.
(39) Allen, M. J.; Tung, V. C.; Kaner, R. B. Honeycomb Carbon: A Review of Graphene. *Chem. Rev.* **2010**, *110*, 132−145.
(40) Yang, J.; Winter, M.; Besenhard, J. O. Small Particle Size Multiphase Li-Alloy Anodes for Lithium-Ion Batteries. *Solid State Ionics* **1996**, *90*, 281−287.
(41) Debart, A.; Dupont, L.; Poizot, P.; Leriche, J. B.; Tarascon, J. M. A Transmission Electron Microscopy Study of the Reactivity Mechanism of Tailor-Made CuO Particles toward Lithium. *J. Electrochem. Soc.* **2001**, *148*, A1266−A1274.
(42) Xue, X. Y.; Chen, Z. H.; Xing, L. L.; Yuan, S.; Chen, Y. J. SnO_2/α-MoO_3 Core-Shell Nanobelts and Their Extraordinarily High Reversible Capacity as Lithium-Ion Battery Anodes. *Chem. Commun.* **2011**, *47*, 5205−5207.